

Secondary Organic Aerosol Formation during the Photooxidation of Toluene: NO_x Dependence of Chemical Composition

Kei Sato,* Shiro Hatakeyama,† and Takashi Imamura

National Institute for Environmental Studies, 16-2, Onogawa, Tsukuba, Ibaraki 305-8506, Japan

Received: February 19, 2007; In Final Form: June 18, 2007

The photooxidation of toluene is a potential source of secondary organic aerosol (SOA) in urban air, but only a small portion of the compounds present in SOA have been identified. In this study, we analyzed the chemical compositions of SOA produced by photoirradiation of the toluene/NO_x/air system in laboratory chamber experiments by a combination of liquid chromatography–mass spectrometry, hybrid high-performance liquid chromatography–mass spectrometry, and iodometry–spectrophotometry. The dependence of the chemical composition on the initial NO_x concentration was examined at initial NO concentrations ([NO]₀) of 0.2 and 1 ppmv. Fifteen semivolatile products, including aromatic and ring-cleavage compounds, were quantified. However, the quantified products comprised only a small portion (~1 wt %) of the total aerosol mass. The total SOA yield (~13 wt %), the ratio of organic peroxides to total SOA mass (~17 wt %), and the density of SOA (~1.4 g cm⁻³) were independent of the NO_x level, suggesting that the reaction mechanisms of the formation of major SOA products at [NO]₀ = 0.2 and 1 ppmv are essentially the same. The negative-ion mass spectra of SOA samples showed that ion signals attributed to hemiacetal oligomers and/or decomposition products of peroxy hemiacetal oligomers were detected in the range of mass-to-charge ratios (*m/z*) between 200 and 500. The highest signals were detected at *m/z* = 155 and 177, and these were tentatively assigned to C₇ unsaturated oxacyclic oxocarboxylic acids and C₇ unsaturated oxacyclic dicarboxylic acids, respectively. We conclude that the major chemical components of the aerosol are hemiacetal and peroxy hemiacetal oligomers and low-molecular-weight dicarboxylic acids.

1. Introduction

Toluene is a potential source of photochemical ozone and secondary organic aerosol (SOA) in urban air.^{1,2} To evaluate SOA formation potentials under various physical and chemical conditions in the troposphere, an understanding of gas-phase reaction mechanisms of SOA formation is required.³ The oxidation of toluene in the presence of NO_x is initiated by reaction with OH radicals. The reaction with OH radicals proceeds through the addition of OH to the benzene ring (94%) or the abstraction of hydrogen from the methyl group by OH radicals (6%), as shown in Figure 1. The primary radical products, an OH–aromatic adduct (product b in Figure 1) and a benzyl radical (product a in Figure 1), are oxidized by subsequent rapid reactions to form first-generation products (P, P', and P'' in Figure 1). These first-generation products are stable molecules produced directly by the gas-phase oxidation of toluene. Odum et al., who introduced a gas–particle absorptive partitioning model for the formation of SOA, assumed that the products contributing to SOA formation were first-generation products from the oxidation of toluene.⁴ Later workers, however, pointed out, on the basis of comparisons of total SOA concentrations measured by chamber experiments with predictions from chemical-reaction models, that second-generation products also contribute to the formation of SOA.^{5–8} These second-generation products are stable molecules produced by gas-phase oxidation of the first-generation products. Hurley et

al. measured SOA concentrations as a function of toluene consumption at various initial NO_x and toluene concentrations. They interpreted the experimental results obtained in the region of [NO_x]₀/[toluene]₀ ≥ 1 (where [NO_x]₀ and [toluene]₀ are the initial concentrations of NO_x and toluene, respectively) by assuming that compounds produced by reactions of first-generation products with OH radicals contributed to SOA formation⁶ (reaction Scheme 1)



Here, P represents first-generation products that react with OH radicals, and S represents low-volatility second-generation products. However, the experimental results for [NO_x]₀/[toluene]₀ ≤ 1 could not be explained in terms of reaction scheme 1. Hurley et al. suggested that compounds contributing to SOA formation were produced by reactions of first-generation products with OH radicals, O₃, and/or NO₃ radicals. Recently, Sato et al. studied SOA formation in the region of [NO_x]₀/[toluene]₀ ≤ 1, and they noted that the concentration of SOA increased above the detection limit when the rate of formation of photochemical ozone reached a maximum.⁷ They also showed that the concentrations of SOA could be explained by assuming that products contributing to the formation of SOA were produced by reactions of alkene-type first-generation products with O₃ (reaction scheme 2A)



* Author to whom correspondence should be addressed. E-mail kei@nies.go.jp.

† Present address: Tokyo University of Agriculture and Technology, Saiwai-cho, Fuchu, Tokyo 183-8509, Japan.

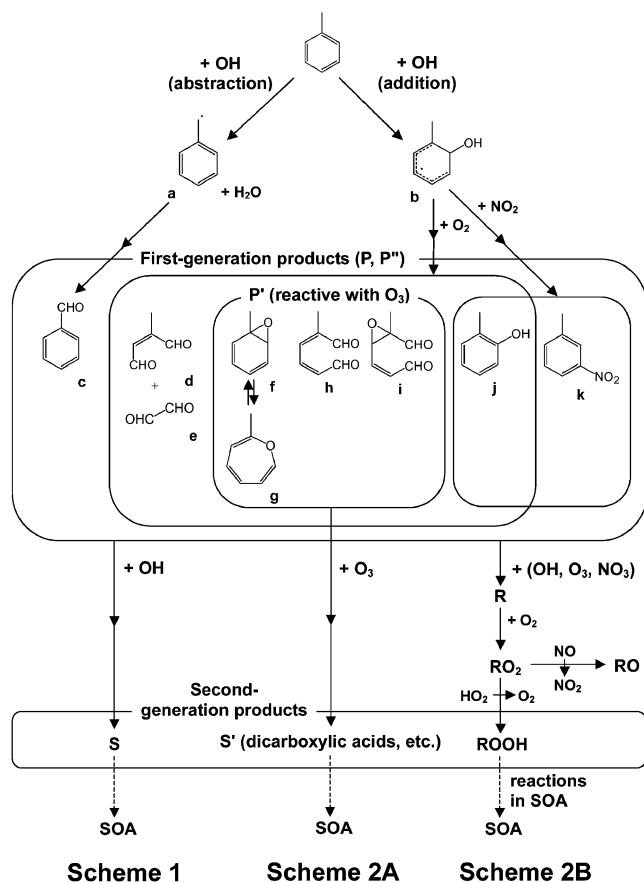
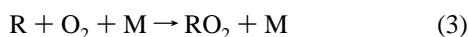
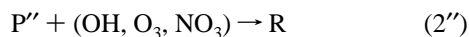


Figure 1. Assumed mechanisms of SOA formation during the photooxidation of toluene. Primary products (a, benzyl radical; b, OH-toluene adduct) and first-generation products (c, benzaldehyde; d, 2-methylbutenedial; e, glyoxal; f, toluene oxide; g, 2-methyloxepin; h, 2-methylmuconaldehyde; i, C₇ unsaturated epoxy dialdehyde; j, *o*-cresol; k, 3-nitrotoluene) are also shown.

Here, P' represents first-generation products that react with O₃, and S' represents low-volatility second-generation products (e.g., oxocarboxylic acids and dicarboxylic acids). However, Johnson et al. checked available experimental data in their modeling study and pointed out that the concentration of SOA increased above the detection limit when the concentration of NO decreased below the detection limit.⁸ They assumed that organic peroxides (ROOH, R = organic group) produced by the reactions of organic peroxy radicals (RO₂) with HO₂ radicals contributed to the formation of SOA. They explained the suppression of the formation of SOA in the presence of NO in terms of removal of RO₂ radicals by reactions with NO (reaction scheme 2B)



Here, P' represents first-generation products that react with OH radicals, O₃, and/or NO₃ radicals to form RO₂ intermediates, and M represents a third-body molecule. Although both reaction

schemes 2A and 2B include reactions of first-generation products with O₃, the assumed low-volatility compounds are different.

We attempted to verify the gas-phase reaction schemes proposed by previous workers by analyzing the chemical composition of SOA. Ring-containing products produced by the oxidation of toluene (such as nitrophenols and benzoic acid) and ring-cleavage products (such as carboxylic acids, carbonyl compounds, and anhydrides) have been identified as components of SOA produced by using gas chromatography–mass spectrometry (GC-MS).^{9–12} However, the GC-MS method is unsuitable for the analysis of low-volatility compounds and pyrolytic compounds,¹³ so products comprising only about 10% of the total mass of SOA can be identified by using this technique.¹² Less-volatile hemiacetal oligomers have recently been identified in SOA from the photooxidation of 1,3,5-trimethylbenzene by using matrix-associated laser desorption ionization–mass spectrometry (MALDI-MS).¹⁴ However, molecular-level analysis by using MALDI-MS is difficult at present. Liquid chromatography–mass spectrometry (LC-MS), however, is suitable for molecular-level analysis of low-volatility compounds. Carboxylic acids,^{15,16} nitrophenols,¹⁷ products of hydrolyses of anhydrides,¹⁸ and dibutylamine (DBA) derivatives of anhydrides¹⁹ can be analyzed by using an LC-MS method. Newly identified products have been successfully characterized by LC-MS methods combined with high-resolution mass spectrometry, a collision-induced dissociation (CID) method, and derivatization by Girard's reagent P (Gir-P; 1-(2-hydrazino-2-oxoethyl)-pyridinium chloride).^{15,20} Because organic peroxides dissociate on the surface of metal materials, these compounds cannot be detected by using an LC-MS method. The total amounts of organic peroxides in SOA can, however, be quantified by using an iodometric–spectrophotometric method.^{20,21}

In this study, products contained in SOA produced by oxidation of toluene were analyzed by using an LC-MS method. The dependence of the product distribution on the NO_x concentration was determined by quantitative analysis of known products. Newly found products were characterized by using LC–high-resolution mass spectrometry, a CID method, and a Gir-P derivatization method. The total amounts of organic peroxides were quantified by an iodometric–spectrophotometric method. The aims of this work were to elucidate the dependence of chemical composition on the NO_x concentration and to verify the previous gas-phase reaction schemes for SOA formation produced by chemical composition analysis.

2. Experimental Methods

2.1. Chamber Experiments. Nine experiments were conducted (Table 1) by using a 6 m³, temperature-controllable, Teflon-coated, stainless-steel chamber^{22,23} in the absence of seed particles. The initial toluene and initial NO concentrations were 4 and 1 ppmv, respectively in runs 1, 3, 5, and 9. In the other runs, the initial toluene concentration was kept at 4 ppmv, whereas the initial NO concentration was set to 0.2 ppmv. Purified and filtered air was used as a dilution gas. Total pressures were 1002–1030 hPa. A small amount of methyl nitrite (~10 ppbv) was added to the reaction mixture as a source of OH radicals. The reaction mixture was irradiated by light from xenon arc lamps (19 kW) through Pyrex filters. The photolysis rate of NO₂ was $(4.7 \pm 0.2) \times 10^{-3} \text{ s}^{-1}$. The concentrations of toluene, NO, NO₂, and O₃ were monitored by using a Fourier transform infrared (FT-IR) spectroscope (Nicolet, Nexus 670) combined with a mirror system with a 221.5 m optical path.²⁴ The volume concentration of SOA (V)

TABLE 1: Initial Conditions, Irradiation Duration, Results of Toluene Consumptions, and Results of Aerosol Concentrations of All Experiments

run	[toluene] ₀ ^a (ppbv)	[NO _x] ₀ ^a (ppbv)	irradiation duratio (h)	Δtoluene ^b (μg m ⁻³)	ΔVc ^b (μm ³ cm ⁻³)	(V) ^c (μm ³ cm ⁻³)	collected aerosol mass (μg)	M ₀ (μg m ⁻³)	note
run 1	4014	1027	5.0	3986	374	264	403	392	ISP ^d
run 2	3980	199	3.0	1675	166	99	257	127	ISP ^d
run 3	4026	1014	4.5	4123	343	210	557	278	LC-MS
run 4	4004	207	3.0	1730	156	92	207	97	LC-MS
run 5	3982	1011	4.5	4069	366	244	663	325	LC-MS
run 6	3998	208	3.0	1567	131	77	190	92	LC-MS
run 7	4074	210	8.0	2394	246	85	223	109	LC-MS
run 8	4005	210	3.0	1647	132	81	213	104	LC-MS (Gir-P)
run 9	3824	1000	4.5	3964	400	237	660	327	LCMS-IT-TOF

^a Initial experimental conditions. ^b Results of the final measurement during irradiation. ^c Results of average during sampling. ^d Iodometric–spectrophotometric method.

was measured by using a scanning mobility particle sizing (SMPS; TSI, 3934). SOA particles were collected at a flow rate of 0.3 L min⁻¹ through a 60 cm stainless-steel tube with a 0.25 in. outer diameter. Irradiation was continued until the volume concentration of SOA leveled off. The durations of irradiation of the experiments conducted at [NO]₀ = 0.2 and 1 ppmv were generally 3.0 and 4.5 h, respectively. The duration of irradiation in run 7 was extended to 8 h to study the temporal dependence of the product distribution. The initial temperature of the chamber wall was controlled at 298 ± 1 K. Although the temperature increased with irradiation time, the total temperature increase during irradiation was less than 2 K. The wall-deposition loss rates of SOA were measured by monitoring the SOA concentration in the dark after conclusion of the experiments. An excess of NO was introduced to suppress further O₃ and NO₃ radical reactions. The wall loss rate was determined to be 5 × 10⁻⁵ s⁻¹. The volume concentrations measured by SMPS were converted to corrected volume concentrations (V_c) by taking into account the measured wall loss rate.

Toluene (99%), dibutylamine (98%), Girard's reagent P (for biochemistry), formic acid (for HPLC), acetic acid (for HPLC), distilled water (for HPLC), methanol (for HPLC), dichloromethane (for HPLC), ethyl acetate (for HPLC), chloroform (for HPLC), and potassium iodide (99.5%, for oxidant analysis) were purchased from Wako Chemicals and used without purification. Benzoyl peroxide (40 wt % in dibutyl phthalate) and 22 standard compounds (>98%) for quantifications of products (described later) were purchased from Sigma-Aldrich and used without purification. Nitric oxide (Takachiho Chemical Industrial Co., 99.9%) was used after vacuum distillations to remove any nitrogen dioxide impurity. Nitrogen dioxide (Sumitomo Seika Co.) was used after vacuum distillations to remove any nitric oxide impurity. Methyl nitrite was prepared by dropping 50 wt % aqueous sulfuric acid (Kanto Chemical Co., 97–98%) onto methanolic sodium nitrite (Wako Chemicals, 98.5%) and was used after vacuum distillation to remove any methanol impurity.

2.2. Sample Collections and Pretreatments. After the xenon lamps had been turned off, the air from the chamber was collected by using a low-volume air sampler (Shibata, LV40B) at a flow rate of 16.7 L min⁻¹ for 1–2 h through a 60 cm stainless-steel tube with a 0.5 in. outer diameter. SOA particles were collected on a Teflon membrane filter (Sumitomo Electric, 47 mm diameter, 1 μm pore size) inserted downstream of the collection tube. Purified air was injected into the chamber at 17.0 L min⁻¹ during sampling to maintain a constant pressure in the chamber. The filter was weighed by using an electric microbalance (Mettler Toledo, AG285); average results from three gravimetric measurements were used. The total mass of

collected SOA was determined from the difference between the weight of the filter after sampling and that before sampling. The sample filter was placed in a 20 mL vial and stored at -15 °C until required for pretreatment. The pretreatments and analysis were conducted within 24 h of sampling.

The procedure for pretreatment in runs 3, 4, 5, 6, 7, and 9 was as follows. The filter was cut into small pieces and sonicated in 3 mL of dichloromethane for 20 min. A 1.6 mL fraction of the extract was placed in a 5 mL vial and concentrated to near dryness under a gentle stream of nitrogen. The concentrated sample was dissolved in 100 μL of methanol/formic acid/water (20:0.04:79.96 v/v/v) solution. The solution was sonicated for 10 min and then used for analysis. Another 0.8 mL fraction of the extract was placed in a 5 mL vial and used for DBA derivatization analysis.¹⁹ Derivatization of anhydrides ($M = M'$) with DBA gave the corresponding amides ($M = M' + 129$) (where M is the molecular weight). A 0.02 M solution of DBA in dichloromethane (0.8 mL) was added to the 0.8 mL fraction of the extract, and the mixture was sonicated for 20 min, then concentrated to near dryness. The concentrated mixture was dissolved in 100 μL of methanol, and the methanolic solution was used as an analytical sample after sonication for 10 min.

2.3. LC-MS Analysis. A sample (5–50 μL) was injected into an LC-MS instrument²⁵ (Shimadzu, QP-8000α). Methanol and 0.05% aqueous formic acid were used as eluents. Formic acid, which has a higher acidity than acetic acid, was used as a buffer to reduce the retention times of nitrophenols. The total flow rate of the eluents was 0.4 mL min⁻¹. The concentration of methanol was kept constant at 20% in the flow-injection analysis in which no column is used. In column-injection analysis, an octadecyl column (GL Science, Inertsil ODS-3, 3.0 mm × 150 mm, 3 μm particle size) kept at 35 °C was used for the separation of the analytes. The methanol concentration was programmed to be 20% (0–5 min), 20–90% (5–25 min), 90% (25–45 min), and 20% (45–60 min). Analytes were ionized by an atmospheric-pressure chemical ionization (APCI) method. Sample eluent was nebulized from an APCI probe heated to 400 °C by using nitrogen at a flow rate of 2.5 L min⁻¹ as the nebulizing gas. Charged droplets produced by the APCI probe were introduced into a vacuum chamber through a curved desolvation line heated to 250 °C. Ions emerging from the desolvation line were focused by a deflector and then introduced into a quadrupole mass spectrometer (QMS). The voltages of the APCI probe, the desolvation line, and the deflector were optimized at 4500, -20, and 30 V, respectively, in the positive-ion ((+)APCI) mode and at -3000, 30, and -20 V, respectively, in the negative-ion ((-)APCI) mode. A region of mass-to-charge ratios (m/z) below 1000 or 500 was scanned at a rate of 500 or 250 Da s⁻¹, respectively. To obtain higher signal-to-

TABLE 2: Structure, Retention Times (RTs), and m/z of Abundant Ions of Standard Compounds

no.	molecules	structure	RT / min	m/z		note
				(+)APCI	(-)APCI	
aromatic compounds						
1	2-hydroxy-5-nitrobenzaldehyde		25.8	110 ($M-57$), 124 ($M-43$), 138 ($M-29$), 170 ($M+3$)	166 ($M-1$)	<i>a,b,c</i>
2	benzoic acid		26.5	no signal	121 ($M-1$), 167 ($M+45$)	<i>a,b,c</i>
3	4-nitro- <i>m</i> -cresol		28.7	122 ($M-31$), 124 ($M-29$), 156 ($M+3$)	136 ($M-17$), 152 ($M-1$)	<i>a,b,c</i>
4	4-nitro- <i>o</i> -cresol		29.9	122 ($M-31$), 124 ($M-29$), 156 ($M+3$)	136 ($M-17$), 152 ($M-1$)	<i>b,c</i>
5	2-nitro- <i>p</i> -cresol		32.2	124 ($M-29$), 156 ($M+3$)	no signal	<i>a,b,c</i>
6	3-nitrotoluene		32.5	108 ($M-29$), 140 ($M+3$)	no signal	<i>b,c</i>
7	4,6-dinitro- <i>o</i> -cresol		33.4	137 ($M-61$), 139 ($M-59$)	181 ($M-17$), 197 ($M-1$), 198 (M)	<i>b,c</i>
carboxylic acids						
8	malic acid		3.2	no signal	133 ($M-1$)	<i>d</i>
9	succinic acid		3.4	no signal	117 ($M-1$)	<i>e</i>
10	levulinic acid		4	117 ($M+1$), 131 ($M+15$), 149 ($M+33$)	113 ($M-3$), 115 ($M-1$), 161 ($M+45$)	<i>a</i>
11	malonic acid		4.6	no signal	103 ($M-1$)	<i>d</i>
12	pyruvic acid		5.8	no signal	87 ($M-1$), 133 ($M+45$)	<i>b</i>
13	2-oxoglutaric acid		6.8	no signal	145 ($M-1$)	<i>d</i>
14	muconic acid		8.3	no signal	141 ($M-1$), 187 ($M+45$)	<i>d</i>
15	maleic acid		10.4	no signal	115 ($M-1$)	<i>e</i>
16	citraconic acid		12.9	no signal	129 ($M-1$)	<i>e</i>
carbonyls						
17	Acetylacetone		5.4	115 ($M+1$), 129 ($M+15$), 147 ($M+33$)	no signal	<i>f</i>
18	α -angelicalactone		9.5	99 ($M+1$), 131 ($M+33$)	no signal	<i>a,b</i>
19	5-methylfurfural		15	111 ($M+1$), 125 ($M+15$), 143 ($M+33$)	no signal	<i>b,c</i>
dibutylamine derivatives of anhydrides						
20	maleic anhydride		32.5	130 ($M+32$), 184 ($M+86$), 228 ($M+130$)	226 ($M+128$), 272 ($M+174$)	<i>a,b,c</i>
21	succinic anhydride		32.8	130 ($M+30$), 230 ($M+130$), 244 ($M+144$)	no signal	<i>a,b</i>
22	citraconic anhydride		33.5	130 ($M+18$), 198 ($M+86$), 242 ($M+130$)	240 ($M+128$), 286 ($M+174$)	<i>a,b,c</i>

^a Products found by Hamilton et al.¹² ^b Products found by Jang and Kamens (including both gas- and particle-phase products as defined in their paper).¹⁰ ^c Products found by Forstner et al.⁹ ^d Analogues of carboxylic acids found by Jang and Kamens.¹⁰ ^e Products of hydrolyses of anhydrides. ^f Analogue of polyketones found by Edney et al.¹¹

noise ratios, 64 selected ions were also monitored at a scan rate of 32 Da s⁻¹; this number of selected ions is the upper limit for the present instrument operated in this selected-ion monitoring (SIM) mode. Ions used for quantifications and other abundant ions were selected. The ions from a mass filter were detected by using a secondary electron multiplier. A mass spectrum was obtained every 2 s by integrating the output signals for 2 s. To study the structures of the analytes, fragment ions produced by CID processes were also observed in the (-)APCI mode for separated chromatographic peaks. The voltages of the desolvation line and the deflector were set to 10 and -70 V, respectively. Under these conditions, ions produced by APCI processes were dissociated by collisions with neutral molecules in the deflector. To check total recoveries of carboxylic acids in the present method, 10 μ L of a solution of malic acid (2 μ g μ L⁻¹) in dichloromethane was spiked on a Teflon filter, and the filter was analyzed. The recovery was confirmed to be >90%, suggesting that carboxylic acids are successfully ex-

tracted by using dichloromethane as the solvent. A blank sample was prepared by collecting purified air passed into the chamber thorough a Teflon filter. It was confirmed that no chromatographic peak was detected by LC-MS analysis of the blank sample.

Twenty-two selected compounds were analyzed as standard molecules for aromatic and ring-cleavage products (Table 2). Of these selected compounds, 14 are known products from previous GC-MS studies.⁹⁻¹² Malic acid, malonic acid, 2-oxoglutaric acid, and muconic acid are analogues of multifunctional carboxylic acids identified as products by Jang and Kamens.¹⁰ Maleic acid, succinic acid, and citraconic acid are products of hydrolyses of anhydrides. Acetylacetone is an analogue of the polyketones identified by Edney et al.¹¹ The three anhydrides were analyzed after derivatization by DBA, whereas the other 19 compounds were analyzed without derivatization. The mass spectra of the 19 compounds and 3 derivatives were measured by an electrospray ionization (ESI) method as well as by the

APCI method. The retention times and the calibration curves were measured by using the APCI method. The concentrations of external-standard samples used for calibration purposes were 0, 10, 20, and 50 ng μL^{-1} .

2.4. Gir-P Derivatization. Products containing carbonyl groups were analyzed by the Gir-P derivatization method^{20,26} for an SOA sample obtained at $[\text{NO}]_0 = 0.2$ ppmv (run 8). The SOA sample filter was cut into small pieces and sonicated in 3 mL of dichloromethane for 20 min. A 0.8 mL fraction of the extract was concentrated to near dryness. The extract was mixed with Gir-P/acetic acid/methanol solution (2.0 mL; 0.19:0.04:100 w/v/v), and the mixture was heated at 50 °C for 3 h, then concentrated to near dryness. The concentrated mixture was dissolved 100 μL of methanol/formic acid/water (20:0.04:79.96 v/v/v) solution. The solution was sonicated for 10 min and then used for analysis. The derivative sample was analyzed in the (+)APCI mode. Before analysis of the SOA sample, derivatives of pyruvic acid and acetonylacetone were analyzed. Gir-P ($M = 187$) reacts with aldehydes and ketones to form water-soluble hydrazones with a positively charged pyridine moiety, and water is eliminated in this reaction. The organic unit that adds to aldehydes and ketones has a mass of 152 Da. Thus, the reactions of carbonyl compounds ($M = M'$) with Gir-P give ions of $m/z = [M' + n(152 - 18)]/n$ (where n is the number of carbonyl groups). The derivatives of pyruvic acid with one carbonyl group ($M = 88$) and acetonylacetone with two carbonyl groups ($M = 114$) were detected as singly charged ions at $m/z = 222$ and doubly charged ions at $m/z = 191$, respectively.

2.5. LCMS-IT-TOF Analysis. High-resolution mass analysis was conducted by using a hybrid high-performance liquid chromatograph–mass spectrometer (Shimadzu, LCMS-IT-TOF) to determine the chemical formulas of the products. The SOA sample obtained at $[\text{NO}]_0 = 1$ ppmv (run 9) was studied by flow-injection analysis in the (–)APCI mode. Ions of $m/z = 100$ –1000 captured by an ion trap were analyzed by using a time-of-flight mass spectrometer that had a single reflector (~ 1.5 m flight length). The output signals from a multiple-channel plate were measured every 1 ns. The other analytical conditions were essentially the same as those for analysis with the QMS. Before the SOA sample was analyzed, a mass calibration was conducted. It was confirmed that masses of 4-nitro-*o*-cresol and 4,6-dinitro-*o*-cresol were determined within an error of ± 5 mDa. Possible chemical formulas corresponding to each measured mass within an error of ± 20 ppm were searched by using software (Shimadzu, Formula Predictor Software). In the determinations of the chemical formulas, the measured negative ions were assumed to be ions produced by deprotonation of analyte molecules ($M - \text{H}$ quasi-molecular ions).

2.6. Iodometric–Spectrophotometric Analysis. Iodometric–spectrophotometric analysis²¹ of the SOA sample obtained at $[\text{NO}]_0 = 1$ and 0.2 ppmv (runs 1 and 2, respectively) was carried out immediately after sampling to quantify total amounts of organic peroxides (ROOR and ROOH) in the aerosols. In this analysis, molecular iodine produced by the reactions of organic peroxides with potassium iodide is quantified by spectrophotometry. The quantum yields of iodine from the reactions of various organic peroxides, including hydroperoxides, diacyl peroxides, diaroyl peroxides, peresters, and ketone peroxides, have been confirmed by Banerjee and Budke to be close to 1.²⁷ The sample filter was sonicated in 1.0 mL of ethyl acetate for 20 min. The extract was then mixed with 1.5 mL of acetic acid/chloroform/water (0.53:0.27:0.20 v/v/v) solution. A 2.0 mL fraction of the 2.5 mL of mixture was placed in a 5 mL vial. Nitrogen gas was bubbled gently through the mixture for

5 min to remove dissolved oxygen. The solution was then mixed with 24 mg of potassium iodide. The sample vial was again flushed with nitrogen and then capped. One hour after being mixed with KI, the sample solution was placed in a quartz cell with a 1 cm optical path length. The absorbance of iodine produced in the sample solution was measured at 470 nm by using a UV–vis spectrophotometer (Shimadzu, BioSpec-mini), taking the absorbance of the solvent as a reference. A blank sample was also prepared by using a new filter and analyzed in a similar manner. A calibration curve was obtained by using 0–4.0 mM solutions of benzoyl peroxide in ethyl acetate.

3. Results

3.1. LC-MS Analysis of Standard Samples. An ionization method suitable for detecting the products was identified by recording APCI and ESI mass spectra for the 22 standard compounds at an injection mass of 250 ng. Signals from all of the standard compounds were detected by the APCI method, but no signals for compounds of moderate polarity (compounds 5, 6, 17, 18, and 19) were detected by the ESI method. Therefore, we selected the APCI method as being suitable for the analysis of a wide range of compounds. Table 2 shows the m/z ratios of abundant ions measured in analyses of the standard compounds. The most abundant ions of each compound observed in (+)APCI and (–)APCI modes are underlined.

The compounds detected in the (–)APCI mode were benzoic acid, 4-nitrophenols (compounds 1, 3, 4, and 7), carboxylic acids (compounds 8–16), the DBA derivative of maleic anhydride, and the DBA derivative of citraconic anhydride. The $M - \text{H}$ quasi-molecular ions were the most abundant among the detected ions in the mass spectra of all of the detected compounds. The adduct ions produced by the additions of formate ions were also observed at $m/z = M + 45$ in the mass spectra of three carboxylic acids (compounds 10, 12, and 14).

The compounds detected in the (+)APCI mode were nitrophenols (compounds 1, 3, 4, 5, 6, and 7), levulinic acid, carbonyl compounds (compounds 17–19), and DBA derivatives of anhydrides (compounds 20–22). Positive ions produced by the protonation of analytes ($M + \text{H}$ quasi-molecular ions) were the most abundant ions in the mass spectra of levulinic acid, the carbonyl compounds, and the derivatives of anhydrides. The ion peaks for $m/z = M + 33$ and $M + 15$ were also recorded in the mass spectra of compounds containing carbonyl groups; these ions were attributed to the adduct ions of protonated methanol ($[M + \text{CH}_5\text{O}]^+$) and the dehydration products from the adduct ions ($[M + \text{CH}_5\text{O} - \text{H}_2\text{O}]^+$), respectively. Ions of $m/z = M + 3$ and $M - 29$ were observed in the mass spectra of mononitrophenols (compounds 1, 3, 4, 5, and 6); these ions were attributed to the $[M + \text{CH}_5\text{O} - \text{HCHO}]^+$ and $[M + \text{CH}_5\text{O} - \text{HCHO} - \text{O}_2]^+$ ions, respectively. In the mass spectrum of 4,6-dinitro-*o*-cresol, fragment ions of $m/z = M - 61$ were the most abundant. The quasi-molecular ions were the most abundant except in the case of nitrophenols. The results confirm that stable analytes undergo soft ionization under our selected conditions.

Peak areas of extracted-ion chromatograms (EICs) measured at the underlined m/z values were used for the quantifications of the 22 standard compounds. Standard mixed samples of four different concentrations were analyzed to give calibration curves. The peak areas were plotted as functions of the injected mass. The correlation coefficients (R^2) for all of the compounds were greater than 0.93. The detection limits of the nitrophenols and the derivatives of anhydrides were determined to be < 1 ng by selecting an appropriate mode. The detection limits of the carboxylic acids and the carbonyls were 1–30 ng.

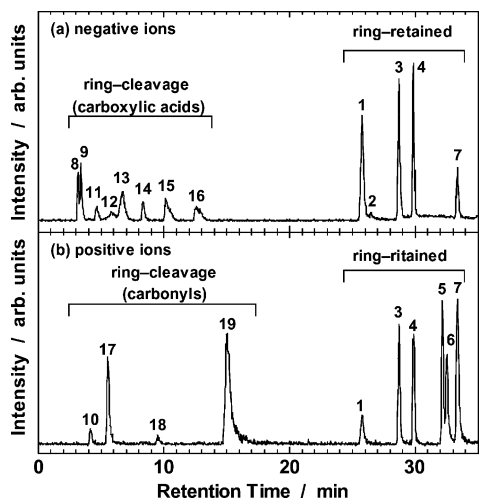


Figure 2. Total ion chromatograms of a standard mixed sample measured in (a) negative-ion mode and (b) positive-ion mode.

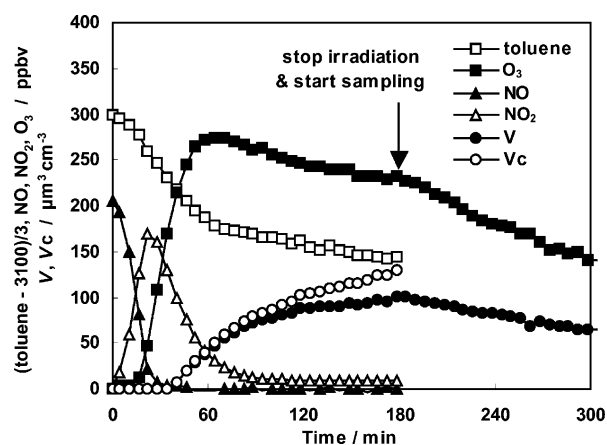


Figure 3. Concentrations of toluene, NO, NO₂, O₃, SOA (V), and SOA (V_c) measured as a function of irradiation time in run 6 ([NO]₀ = 0.2 ppmv).

Figure 2a shows a total ion chromatogram (TIC) of an equimolar mixed sample of compounds 1–19 measured in the (–)APCI mode. The chromatographic peaks of the carboxylic acids were observed within about 17 min, whereas those of the aromatic compounds, including nitrophenols and benzoic acid, were observed after 17 min. In the (+)APCI mode, the chromatographic peaks for carbonyl compounds were observed within 17 min, and those of the aromatic compounds were observed after more than 17 min (Figure 2b). These results suggest that ring-cleavage products elute in 17 min or less and aromatic products elute after 17 min. The retention times of the compounds were determined by averaging results of three measurements (Table 2). The standard deviations of the retention times of all of the compounds were <0.1 s.

3.2. Study of SOA Density by Gravimetric and SMPS Measurements. The concentrations of toluene, NO, NO₂, O₃, SOA (V), and SOA (V_c), measured as a function of time at [NO]₀ = 0.2 ppmv (run 6), are shown in Figure 3. The volume concentration of SOA (V) increased with time and leveled off after 120 min. The xenon lamps were turned off at 180 min, and the SOA sample was then collected. The volume concentration of SOA (V) decreased with time during the sampling. The averaged SOA mass concentration during the sampling (M_0) was determined by dividing the mass of SOA collected on the filter by the total volume of the collected air. The results are summarized in Table 1, together with measured total toluene consumptions (Δ toluene), corrected volume concentrations of

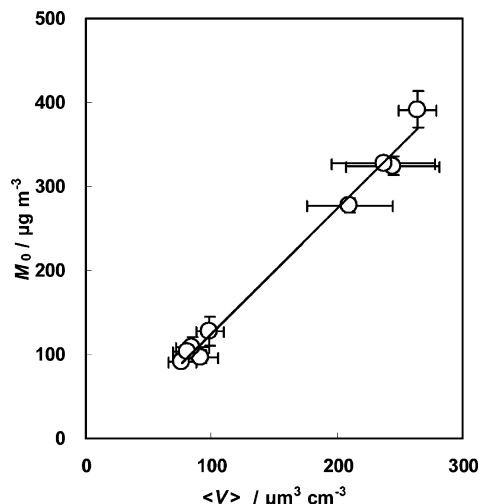


Figure 4. Mass concentrations (M_0) plotted as a function of averaged SMPS volume concentration ($\langle V \rangle$).

the total SOA produced (ΔV_c), averages of measured volume concentrations during sampling ($\langle V \rangle$), and collected aerosol masses. The density of SOA was determined to permit the conversion into mass concentrations of the volume concentrations measured by using SMPS. From the ratio of the SOA mass concentration (M_0) to the volume concentration ($\langle V \rangle$), the average SOA densities at [NO]₀ = 1.0 and 0.2 ppmv were determined to be 1.38 ± 0.07 and 1.22 ± 0.10 g cm⁻³, respectively; the errors are standard deviations. It was found that the SOA density is independent of the initial NO concentration. Therefore, the SOA density in the range of [NO]₀ = 0.2–1 ppmv was determined from a slope of the plot of the mass concentration (M_0) as a function of the volume concentration ($\langle V \rangle$) (Figure 4). The error bars of the mass and volume concentrations in the plot represent the standard deviations of SMPS results during the samplings and those of the three gravimetric measurements, respectively. The correlation coefficient (R^2) of the plot was 0.995. The plotted data were fitted by linear least-squares analysis. The SOA density was determined from the slope of the fitted line to be 1.42 ± 0.08 g cm⁻³; the errors are two standard deviations. The density of SOA often has been assumed to be 1 g cm⁻³,⁴ but we have shown that the density is more than 1 g cm⁻³.

Mass concentrations of the total SOA produced were calculated from the corrected volume concentrations (ΔV_c) by setting the density to be 1.4 g cm⁻³, and these mass concentrations (M_0 (SMPS)) were used for calculations of the mass yields of SOA. The average SOA mass yields ($= M_0$ (SMPS)/ Δ toluene) at [NO]₀ = 0.2 and 1 ppmv were evaluated to be 0.123 ± 0.011 and 0.129 ± 0.010 , respectively. Here, the errors are the standard deviations. The mass yield was independent of the initial NO concentration within experimental uncertainty.

3.3. Mass Spectrometric Analysis of SOA by (–)APCI/LC-MS. Figure 5a shows the mass spectrum of an equimolar solution of compounds 1–19 measured by flow-injection analysis in the (–)APCI mode. The intensities of signals detected in the region of $m/z > 200$ were less than 3% those of the most intense signal at $m/z = 197$. Figure 5b shows a mass spectrum of an SOA sample obtained at [NO]₀ = 0.2 ppmv (run 4). The mass signals of the SOA sample were observed in the region of $m/z = 50$ –500. The most intense peaks were detected at $m/z = 155$ and 171. The TICs of the SOA samples were then measured in the (–)APCI mode by scanning the region of $m/z = 50$ –500. Two broad chromatographic peaks were observed, one within 17 min (early-eluting) and the other

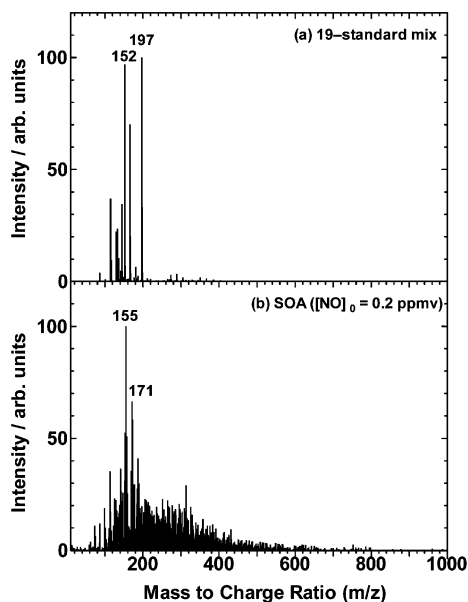


Figure 5. Negative-ion mode mass spectra of (a) standard mixed sample and (b) SOA sample of run 4 ($[\text{NO}]_0 = 0.2$ ppmv). The relative intensities of the most abundant peaks were set to 100.

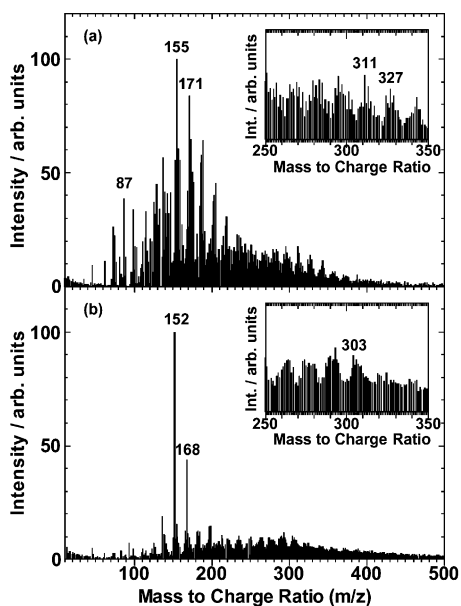


Figure 6. Negative-ion mode mass spectra of run 5 ($[\text{NO}]_0 = 1.0$ ppmv): (a) the early-eluting compounds and (b) the late-eluting compounds. The relative intensities of the most abundant peaks were set to 100.

after 17 min (late-eluting). Early- and late-eluting compounds were found in the TICs of all of the SOA samples. The broad peaks observed were nonseparated chromatographic peaks.

Mass spectra of the SOA sample (run 5) were integrated over the retention time in the ranges corresponding to the early- and late-eluting compounds (Figures 6a and 6b, respectively). In both of the mass spectra, mass peaks were distributed up to $m/z = 500$. The group of peaks in this range showed regular mass differences of 14, 16, and 18. In the mass spectrum of the early-eluting compounds, the most abundant peaks were observed at $m/z = 155$ and 171. The mass peak at $m/z = 87$ is attributed to pyruvic acid ($M = 88$) and its isomers. The most abundant peaks in the mass spectrum of the late-eluting compounds occurred at $m/z = 152$ and 168. The mass peak at $m/z = 152$ is attributed to nitrophenol isomers ($M = 153$). The

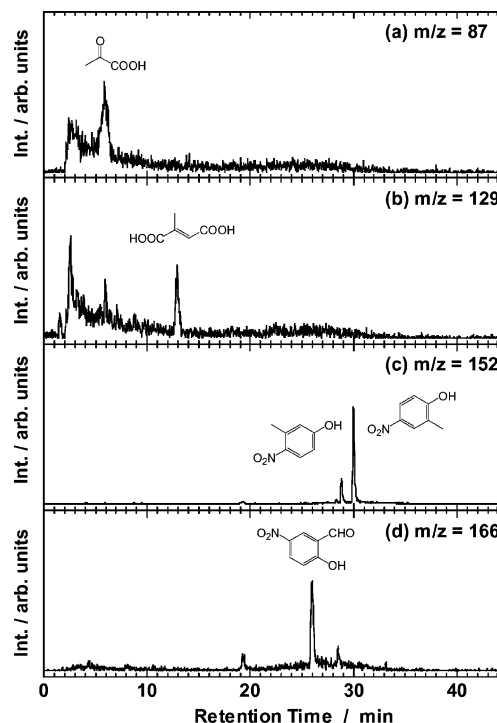


Figure 7. Extracted-ion chromatograms measured in negative-ion mode for the SOA sample of run 5 ($[\text{NO}]_0 = 1.0$ ppmv); ions at (a) $m/z = 87$, (b) $m/z = 129$, (c) $m/z = 152$, and (d) $m/z = 166$. Citraconic acid is the product of hydrolysis of citraconic anhydride (see text).

inner panel is an extended mass spectrum showing the region $m/z = 250$ – 350 . These figures showed that abundant peaks of the early-eluting compounds were detected at $m/z = 311$ and 327, whereas those of the late-eluting compounds were detected at $m/z = 293$ and 303.

3.4. Quantifications of 22 SOA Products in SIM Mode.

Because the chromatographic peaks in TICs were not separated, the selected products were quantified by using EICs measured in the SIM mode at a low mass-scanning rate. Figure 7 shows four typical examples of EICs measured in the ($-$)APCI mode for the SOA samples of run 5. The chromatographic peaks were separated in EICs. By referring to the retention times and mass numbers of standard compounds, the chromatographic peaks at 5.8 min ($m/z = 87$), 12.9 min ($m/z = 129$), 28.7 min ($m/z = 152$), 29.9 min ($m/z = 152$), and 25.8 min ($m/z = 166$) were assigned to pyruvic acid, citraconic acid, 4-nitro-*m*-cresol, 4-nitro-*o*-cresol, and 2-hydroxy-5-nitrobenzaldehyde, respectively. In a similar manner, the chromatographic peaks of 15 compounds were identified. These compounds contained in SOA were quantified by using an external-standard method. Mass percent ratios of the compounds to the total SOA were determined in runs 4–7 (Table 3). Only aromatic compounds were quantified in run 4, whereas all 15 products were quantified in runs 5–7. Total mass ratios of the 15 detected products in runs 5–7 were very small (~ 1 wt %).

Because the signal-to-noise ratios for many chromatograms were low, an uncertainty analysis was carried out. The errors from baseline noises were estimated to be 0.2–60% from the ratios of three standard deviations of noise to peak height. Since the present quantifications were carried out by using the peak areas, these estimations will provide the maximum errors. Not only baseline noise but also errors in the slope of the calibration curves (2–20%) and the errors in the SOA mass concentrations (3–11%) were taken into account. The errors of the mass ratios of the products were then determined by error-propagation analysis. The errors evaluated are also shown in Table 3. Runs

TABLE 3: Mass Ratios of Products to Total SOA in Units of wt %

no.	products	[NO] ₀ = 1 ppmv		[NO] ₀ = 0.2 ppmv	
		run 5	run 6	run 4	run 7
Aromatic Compounds					
1	2-hydroxy-5-nitrobenzaldehyde	0.021 ± 0.002	0.0070 ± 0.0048	0.0065 ± 0.0019	0.0032 ± 0.0021
2	benzoic acid	<0.027	<0.17	<0.064	<0.078
3	4-nitro- <i>m</i> -cresol	0.17 ± 0.03	0.082 ± 0.008	0.071 ± 0.015	0.015 ± 0.002
4	4-nitro- <i>o</i> -cresol	0.68 ± 0.16	0.25 ± 0.03	0.19 ± 0.05	0.087 ± 0.010
5	2-nitro- <i>p</i> -cresol	0.016 ± 0.002	0.0075 ± 0.0018	0.0067 ± 0.0016	0.0036 ± 0.0016
6	3-nitrotoluene	0.0022 ± 0.0016	<0.0050	<0.0037	<0.0046
7	4,6-dinitro- <i>o</i> -cresol	0.015 ± 0.004	<0.0021	0.0020 ± 0.0016	<0.019
Carboxylic Acids					
8	malic acid	<0.017	<0.051		<0.046
9	succinic acid ^a	0.011 ± 0.001	0.035 ± 0.005		0.022 ± 0.004
10	levulinic acid	<0.062	<0.19		<0.35
11	malonic acid	0.056 ± 0.011	0.091 ± 0.021		0.17 ± 0.04
12	pyruvic acid	0.14 ± 0.04	0.31 ± 0.10		0.26 ± 0.09
13	2-oxoglutaric acid	<0.012	<0.038		<0.035
14	muconic acid	<0.0033	<0.011		<0.0096
15	maleic acid ^a	0.030 ± 0.005	0.018 ± 0.012		0.050 ± 0.013
16	citraconic acid ^a	0.037 ± 0.026	<0.077		<0.070
Carbonyls					
17	acetonylacetone	<0.0018	<0.0055		<0.0050
18	α-angelicalactone	<0.044	<0.14		<0.13
19	5-methylfurfural	0.011 ± 0.002	0.042 ± 0.008		0.029 ± 0.006
Dibutylamine Derivatives of Anhydrides					
20	maleic anhydride ^b	0.048 ± 0.009	0.070 ± 0.015		0.044 ± 0.010
21	succinic anhydride ^b	0.040 ± 0.011	0.071 ± 0.021		0.045 ± 0.013
22	citraconic anhydride ^b	0.086 ± 0.025	0.11 ± 0.03		0.074 ± 0.022
total		1.4 ± 0.2	1.1 ± 0.3		0.81 ± 0.41

^a Produced by hydrolysis of anhydrides (see text). ^b Determined on an anhydride-mass basis.

4 and 6 were conducted under the same initial experimental conditions. The mass ratios of each product determined in runs 4 and 6 agreed with each other within the evaluated errors. The products of hydrolyses of anhydrides, i.e., succinic acid, maleic acid, and citraconic acid, were found in the SOA samples. The determined mass ratios of succinic acid were lower than those of the DBA derivative of succinic anhydride. These results imply that the mass yields of the dicarboxylic acids during the hydrolysis of the anhydride products in methanol–water solution are less than 1. The quantified results for DBA derivatives were employed as results for the anhydrides in this study. The mass ratios of the products determined at [NO]₀ = 1 ppmv (run 5) were compared with those determined at [NO]₀ = 0.2 ppmv (run 6). The mass ratios of the aromatic products (compounds 1–7) increased with increasing NO_x concentration, whereas those of the ring-cleavage products (compounds 8–22) decreased with increasing NO_x concentration.

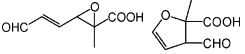
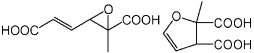
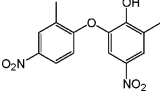
The mass ratios of nitrophenols determined after irradiation for 8 h were lower than those determined after irradiation for 3 h (Table 3), showing that the mass ratios of the nitrocresols decreased with irradiation time. Because the vapor pressure of nitrocresol at a room temperature is estimated to be 2.5×10^{-3} Torr,¹⁰ the gas–particle equilibrium of nitrocresol shifts to the gas-phase side. In the gas phase, photooxidations of nitrocresols are considered to proceed through photolysis.¹ Because the concentrations of nitrocresols in the gas phase decrease as a result of photolysis, the measured mass ratios of nitrocresols decrease following gas–particle absorptive partitioning.

3.5. Determination of Chemical Formulas by LCMS-IT-TOF. Unidentified chromatographic peaks were also found in EICs measured in the (–)APCI mode. To study the unidentified peaks, a high-resolution mass analysis was performed by the LCMS-IT-TOF method. In the measured high-resolution mass spectrum, ion signals were detected in the region of $m/z < 500$,

confirming that peaks detected by using the QMS in the same mass region (Figure 5b) were ion signals rather than noise. Chemical formulas were determined for the mass numbers at which chromatographic peaks were observed in the measurements made by using the QMS. The selected mass numbers, the peak retention times in the EIC, the measured high-resolution masses, the determined formulas, and the tentative identifications are summarized in Table 4. The results were categorized into the early- and late-eluting groups by reference to their peak retention times. The formulas corresponding to the peaks at $m/z = 127, 139, 141,$ and 171 of the early-eluting group agreed with those of carboxylic acids identified as products by Jang and Kamens.¹⁰ The early-eluting compounds detected in the negative-ion mode are attributed to carboxylic acids. The formulas corresponding to the peaks $m/z = 152, 166, 168,$ and 197 of the late-eluting group agreed have been assigned to substituted nitrophenol products.^{9–12}

3.6. (+)APCI/LC-MS and Gir-P Derivatization Analyses for $m/z = 155$ and 171 Products. The chemical formula determined for the product of $m/z = 155$ was C₇H₈O₄ ($M = 156$). The EIC of the $M + H$ quasi-molecular ions ($m/z = 157$) was studied in the (+)APCI mode. The chromatographic peaks were observed at the same retention times as those of the peaks measured in the (–)APCI mode at $m/z = 155$ (Figure 8a). These results imply that the product contains both carbonyl and carboxyl groups. From the chemical formula, the product should contain one or two carbonyl groups and one carboxyl group. To investigate carbonyl compounds contained in the aerosol, the Gir-P derivatives of the products were analyzed. Because all of the Gir-P derivatives in the sample solution eluted within a retention time of 2–3 min, the mass spectrum of the mixture of the derivatives was measured. If the product of $M = 156$ involves one or two carbonyl groups, the ions should be detected at $m/z = 290$ or 212 , respectively. Only ions of $m/z = 290$ were

TABLE 4: High-Resolution Masses Measured by LCMS-IT-TOF Analysis

column injection, LC-QMS		flow injection, LCMS-IT-TOF		
<i>m/z</i> (Da)	RT (min)	<i>m/z</i> (Da)	possible formulas (δ^a) (mDa)	tentative identifications
Early-Eluting Compound				
115	2.4, 5.3, 10.4	115.0024 115.0354	C ₄ H ₄ O ₄ (+0.7) not found	maleic acid ^b
117	2.3, 3.4	117.0215	C ₄ H ₆ O ₄ (-2.7)	succinic acid ^b
127	2.8, 3.8	127.0032 127.0379	C ₅ H ₄ O ₄ (-0.1) C ₆ H ₈ O ₃ (+1.6)	dioxopentenoic acids ^c unidentified
129	2.5, 5.9, 12.9	129.0182	C ₅ H ₆ O ₄ (+0.9)	citraconic acid ^b
139	7.3	139.0393	C ₇ H ₈ O ₃ (+0.2)	methylxohexadienoic acids ^c
141	3.0, 3.5	141.0175	C ₆ H ₆ O ₄ (+1.3)	methylidioxopentenoic acids ^c
155	3.0, 5.7	155.0346	C ₇ H ₈ O ₄ (-0.2)	 C ₇ unsaturated oxacyclic oxocarboxylic acids unidentified
157	5.0, 8.8, 9.1	157.0140 157.0449	C ₆ H ₆ O ₅ (-0.3) not found	unidentified
171	2.9, 3.7, 6.1, 7.0	171.0299	C ₇ H ₈ O ₅ (-0.6)	 C ₇ unsaturated oxacyclic dicarboxylic acids, hydroxydioxoheptenoic acids ^c unidentified
173	3.0, 7.4	173.0433	C ₇ H ₁₀ O ₅ (+1.7)	unidentified
Late-Eluting Compound				
152	28.7, 29.9	152.0346	C ₇ H ₇ NO ₃ (+0.2)	nitrocresols ^{b-e}
166	25.8	166.0171 166.0487	C ₇ H ₅ NO ₄ (-3.1) C ₈ H ₉ NO ₃ (+1.7)	hydroxynitrobenzaldehydes ^{b-e} unidentified
168	19.3, 28.2	168.0300	C ₇ H ₇ NO ₄ (-0.3)	hydroxynitrobenzyl alcohols ^c
197	27.2, 31.4, 33.4	197.0203	C ₇ H ₆ N ₂ O ₅ (-0.5)	dinitrocresols ^{b-d}
221	33.1	221.0493	C ₅ H ₁₀ N ₄ O ₆ (+2.9), C ₁₁ H ₁₀ O ₅ (-4.3) ^f	unidentified
303	37.9	303.0618	C ₁₄ H ₁₂ N ₂ O ₆ (-0.1), C ₁₉ H ₁₂ O ₄ (+3.9), C ₉ H ₁₂ N ₄ O ₈ (-4.1) ^f	 diphenyl-ether-type dimer

^a Determined by subtracting the predicted *m/z* from the measured *m/z*. ^b Produced by hydrolysis of anhydrides (see text). ^c Found by Jang and Kamens.¹⁰ ^d Found by Forstner et al.⁹ ^e Found by Hamilton et al.¹² ^f Formulas satisfying $-5 \text{ mDa} < \delta < 5 \text{ mDa}$ were only listed.

detected, showing that the product molecule contains one carbonyl group. The product was tentatively identified as C₇ unsaturated oxacyclic oxocarboxylic acid isomers as shown in Table 4, taking into account the fact that vinylic alcohols (RCH=C(OH)R') are unstable.

The chemical formula of the product detected at *m/z* = 171 in the (-)APCI mode was determined to be C₇H₈O₅ (*M* = 172). No chromatographic peak was observed in the EIC measured in the (+)APCI mode at *m/z* = 173 (Figure 8b), showing that no carbonyl group was present in the product molecule. The result of Gir-P derivatization analysis confirmed that the product involved no carbonyl group. The product detected at *m/z* = 171 was tentatively assigned to C₇ unsaturated oxacyclic dicarboxylic acid isomers depicted in Table 4. Isomers of C₇H₈O₅ involving two carbonyl groups, the hydroxydioxoheptenoic acids, were identified as products by a previous GC-MS analysis.¹⁰ However, the present results show that these isomers are minor products.

3.7. CID Analysis of the *m/z* = 303 Ion. The peak retention time of the *m/z* = 303 ion was 37.9 min (Table 4). Because the contributions from substances that coelute with the observed chromatographic peaks were negligible in the time region of >30 min, the mass spectrum of this chromatographic peak was measured by using the CID method. Figure 9a shows the mass spectrum of the substance eluting at 37.9 min measured by using the soft ionization method. Mass peaks were detected at *m/z* = 303 and 287. In the mass spectrum measured by the CID method, mass peaks of *m/z* = 256, 167, 152, and 136 appeared

(Figure 9b). The most abundant ions were those at *m/z* = 303 and 152 in the soft ionization method and the CID method, respectively. The results suggest that the product is a dimer (*M* = 304) produced from nitrocresol monomers (*M* = 153). To confirm that the ions of *m/z* = 303 are not adduct ions produced during the ionization processes of nitrocresol monomers, the EICs of *m/z* = 152 (Figure 10a), *m/z* = 303 (Figure 10b), and *m/z* = 305 (Figure 10c) were studied. Nitrocresol monomers eluted at retention times of 28.7 and 29.9 min. The adduct ions produced during the ionization process were detected at a retention time of 29.9 min in the EIC of *m/z* = 305. However, no nitrocresol monomer was eluted with the same retention time as that of the chromatographic peak of *m/z* = 303. The product detected at *m/z* = 303 is a dimer produced in the SOA.

Poly(phenylene ether)²⁸ and phenol-formaldehyde resin²⁹ are known to be produced by solution-phase reactions of phenol monomers. Because the C-C bond dissociations of ions during the CID processes rarely occur, the product is assumed to be a diphenyl-ether-type dimer (methylnitrophenyl hydroxymethyl-nitrophenyl ether), as shown in Table 4. On the basis of this assumption, the ions of *m/z* = 303, 287, 256, 167, 152, and 136 are assigned as [m303]⁻, [m303 - O]⁻, [m303 - HONO]⁻, [m303 - m136]⁻, [m152]⁻, and [m152 - O]⁻, respectively (Figure 9b); the moieties m136, m152, and m303 are shown in the figure. The formula determined for the product detected at *m/z* = 303 (C₁₄H₁₆N₂O₆) satisfies the prediction from high-resolution mass analysis (Table 4). From the results described

above, the chromatographic peak with $m/z = 303$ was tentatively identified as a diphenyl-ether-type dimer.

3.8. Quantification of Peroxides by Iodometry–Spectrophotometry. A calibration curve was obtained by plotting the measured absorbances of iodine produced in benzoyl peroxide solutions as a function of the concentration of benzoyl peroxide ($R^2 = 0.994$). The molar absorptivity was determined to be $829 \pm 59 \text{ L mol}^{-1} \text{ cm}^{-1}$ from the slope obtained by linear least-squares analysis; the error corresponds to two standard deviations. The molar absorptivities measured by Banerjee and Budke,²⁷ Docherty et al.,²¹ and Surratt et al.,²⁰ all using the same technique, were 845, 817, and $852 \text{ L mol}^{-1} \text{ cm}^{-1}$, respectively. The values determined by these previous workers were close to our result. We calculated the mass ratios of organic peroxides to total SOA from the measured absorbances, the mass concentrations of SOA, and the molar absorptivity determined in this study. In the calculations, the average molecular weight of organic peroxides in SOA was assumed to be equivalent to the molecular weight of benzoyl peroxide, because the molecular weight of benzoyl peroxide (242) was close to the average molecular weight determined from the mass spectra measured in the (–)APCI mode for the SOA samples of runs 5–7 (258–286). The mass ratios of organic peroxides to total SOA were determined to be 18 ± 3 and $16 \pm 4 \text{ wt } \%$ at $[\text{NO}]_0 = 1$ and 0.2 ppmv , respectively. The errors were evaluated from the detection limits, the error of molar absorptivity, and the errors of the mass concentrations of SOA.

4. Discussion

4.1. Dependence of SOA Composition on NO_x Concentration. First of all, the present results on the dependence of product distributions on the initial NO_x concentration are discussed from the probable mechanism of the toluene oxidation. In the initial step of the toluene oxidation, an OH–aromatic adduct (product b in Figure 1) is mainly produced by addition of OH to the benzene ring. The OH–aromatic adduct can react with O_2 ($k = 3 \times 10^{-16} \text{ cm}^3 \text{ molecule}^{-1} \text{ s}^{-1}$) or NO_2 ($k = 3 \times 10^{-11} \text{ cm}^3 \text{ molecule}^{-1} \text{ s}^{-1}$).^{30,31} At 2 ppmv NO_2 with ambient O_2 levels, the reactions with O_2 and NO_2 occur at the same rate. With the higher NO_x concentrations in the present study ($[\text{NO}]_0 = 1 \text{ ppmv}$), the reaction of the adduct with NO_2 can compete with the reaction with O_2 . The reaction with NO_2 is believed to result in the formation of cresols and nitrotoluenes (products j and k in Figure 1, respectively) through the formation of an NO_2 adduct, as depicted in reaction scheme 3 of Figure 11.³² This explains the fact that 3-nitrotoluene is only found in the case of $[\text{NO}]_0 = 1 \text{ ppmv}$ in this study. The total yield of cresols from the oxidation of toluene is higher than that of nitrotoluenes between $[\text{NO}_2]_0 = 0$ and 10 ppmv .³⁴ Nitrocresols found in SOA at high NO_x concentrations are believed to be produced through reactions of OH radicals with cresols produced by the reaction of the OH–aromatic adduct with NO_2 .^{9,10} Reactions between OH radicals and cresols form methylphenoxy radicals. NO_2 adds to the benzene ring of methylphenoxy radicals to form adducts, and nitrocresols are produced by the isomerization reactions of these adducts. In a similar manner, dinitrocresols found in SOA can be produced by the reaction of nitrocresols with OH radicals in the presence of NO_2 .^{9,10} The aromatic products detected in high abundances at $[\text{NO}]_0 = 1 \text{ ppmv}$ (Table 3) are formed through the reaction of the OH–aromatic adduct with NO_2 .

At $[\text{NO}]_0 = 0.2 \text{ ppmv}$, the OH–aromatic adduct reacts with O_2 to form an O_2 -bridged cyclic intermediate radical (reaction scheme 4 in Figure 11). Major products of this reaction channel are 2-methylbutenedial (product d in Figure 1) + glyoxal

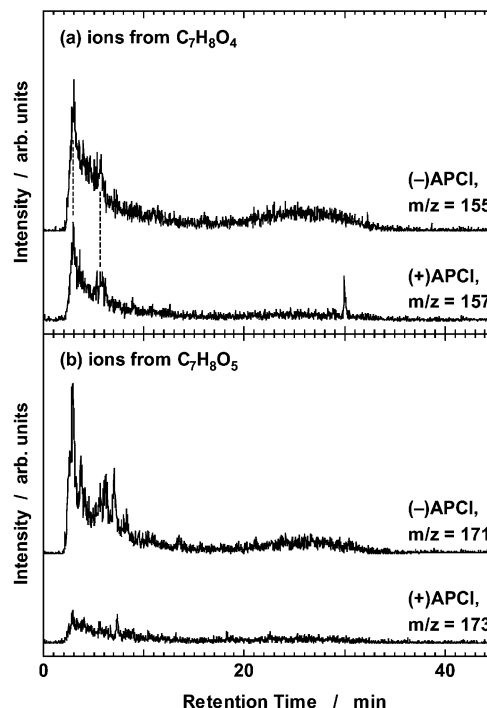


Figure 8. Extracted-ion chromatograms of ions from (a) $\text{C}_7\text{H}_8\text{O}_4$ and (b) $\text{C}_7\text{H}_8\text{O}_5$ products in SOA sample of run 8 ($[\text{NO}]_0 = 0.2 \text{ ppmv}$). The relative intensities of all of the chromatograms were determined by using the same scaling factor.

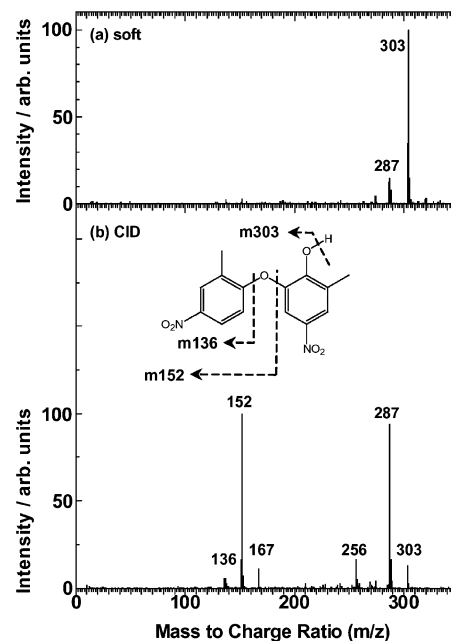


Figure 9. Mass spectra measured for the compound eluting at 37.9 min in the analysis of the SOA sample of run 3 ($[\text{NO}]_0 = 1.0 \text{ ppmv}$): (a) soft ionization method and (b) collision-induced-dissociation method. The intensities of the most abundant peaks were set to 100.

(product e in Figure 1) and butenedial + methylglyoxal. Maleic anhydride found in SOA is believed to be produced by the photolysis of butenedial or by its reaction with OH radicals.^{9,10} The acyl radical ($\text{OHCCH}_2=\text{CH}_2\text{C}(\bullet)\text{O}$) produced by these reactions undergoes subsequent oxidation reactions to form an acyloxy radical ($\text{OHCCH}_2=\text{CH}_2\text{C}(\text{O})\text{O}\bullet$). Maleic hydride is then produced through the abstraction of hydrogen from this acyloxy radical by O_2 . In a similar manner, citraconic anhydride can be produced by the photolysis of 2-methylbutenedial or by its

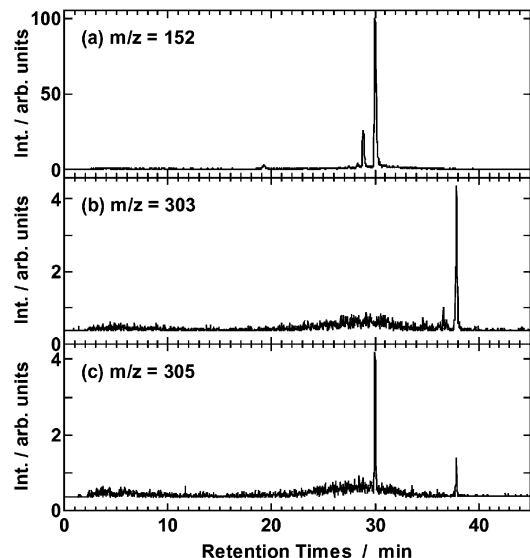
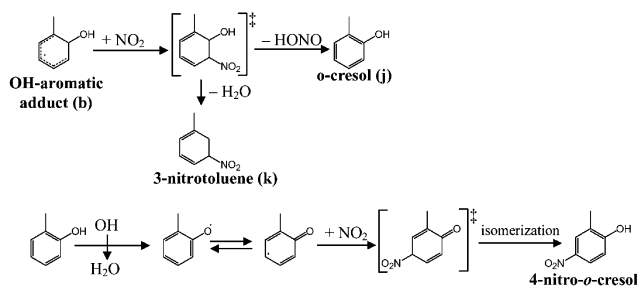
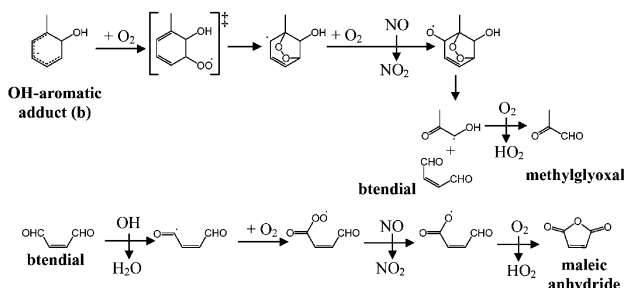


Figure 10. Extracted-ion chromatograms measured by using negative-ion mode for SOA sample of run 3 ($[\text{NO}]_0 = 1.0$ ppmv); ions at (a) $m/z = 152$, (b) $m/z = 303$, and (c) $m/z = 305$. The intensity of the highest peak of $m/z = 152$ was set to 100. The intensities of all of the panels were determined by using the same scaling factor.

Scheme 3 (4-nitro-*o*-cresol formation at high NO_x conditions)



Scheme 4 (Maleic anhydride formation at low NO_x conditions)



Scheme 5 (One of possible reactions to form pyruvic acid)

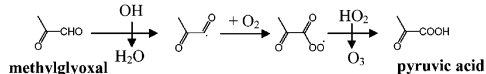


Figure 11. Reaction mechanisms for formation of 3-nitrotoluene, 4-nitro-*o*-cresol, maleic anhydride, and pyruvic acid.

reaction with OH radicals.⁹ Pyruvic acid found in SOA can result from oxidations of various ring-cleavage products.¹⁰ For example, this product results from the reaction of methylglyoxal with OH radicals (reaction scheme 5 in Figure 11). The abstraction of hydrogen by OH radicals from methylglyoxal forms the $\text{O}(\text{CH}_3)\text{CC}(\text{O})\bullet$ radical. This radical is converted to $\text{O}(\text{CH}_3)\text{CC}(\text{O})\text{OO}\bullet$ radical in the presence of excess O_2 . Pyruvic acid is then produced by the reaction $\text{O}(\text{CH}_3)\text{CC}(\text{O})\text{OO}\bullet + \text{HO}_2$

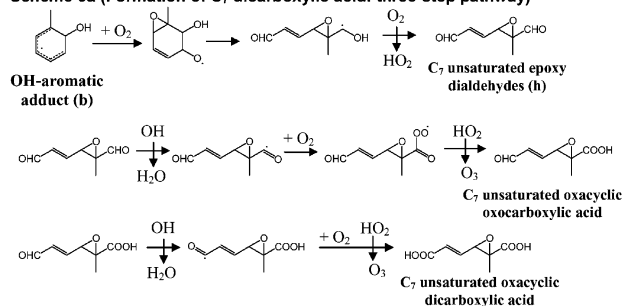
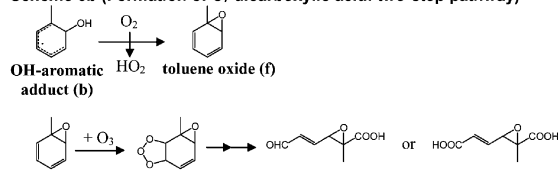
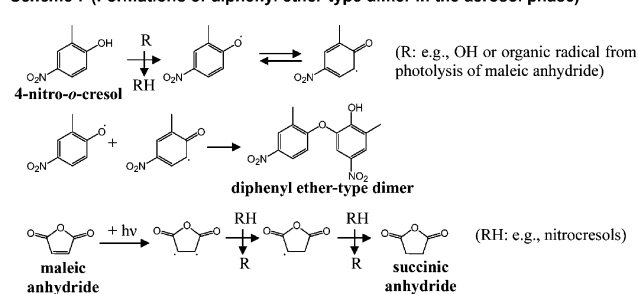
$\rightarrow \text{O}(\text{CH}_3)\text{CCOOH} + \text{O}_3$. The fact that ring-cleavage products are abundant at $[\text{NO}]_0 = 0.2$ ppmv (Table 3) confirms that the toluene oxidation proceeds through the reaction of the OH-aromatic adduct with O_2 at this NO_x concentration. As discussed above, the reactions of the OH-aromatic adduct with O_2 and NO_2 explain our results in terms of the product distribution.

The results of the quantitative analysis showed that compounds with high vapor pressures (e.g., nitrocresols and pyruvic acid) are found in high abundances. Because these products exist mainly in the gas phase at room temperature, the products quantified in this study could be mainly absorbed from the gas phase on the collected aerosols during filter sampling. If this is the case, then the present results on the product distribution are affected by those of the gas-phase products. Further, the products quantified in this study comprised only a small portion (~ 1 wt %) of the aerosol. Although our quantitative analysis results provide information on the overall gas-phase chemistry, these results do not provide information on the formation of major SOA products. In contrast to the dependence of the product distribution on the initial NO concentration, the total SOA yield, the ratio of organic peroxides to total SOA, and the density of SOA were independent of the initial NO concentration in this study. These results suggest that the reaction mechanisms for the formation of major SOA products between $[\text{NO}]_0 = 0.2$ and 1 ppmv are basically the same. The reaction channel contributing to the formation of major SOA products at both the NO_x levels is the reaction of the OH-aromatic adduct with O_2 .

4.2. Previous Reaction Schemes for SOA Formation.

Hurley et al. proposed reaction scheme 1 on the basis of experiments conducted at extremely high NO_x concentrations ($[\text{NO}_x]_0 = 5\text{--}13$ ppmv).⁶ Under these conditions, the reaction of the OH-aromatic adduct with NO_2 is a major reaction pathway during the oxidation of toluene. Nitrocresols are produced as the second-generation products, in accordance with reaction scheme 1. The products of aerosol-phase reactions of nitrocresols (discussed later) will contribute to SOA formation under these conditions. Because the NO_x concentrations examined in this study were much lower than 5 ppmv, we will not discuss this reaction scheme any further in this study.

Our results from the iodometric-spectrophotometric method showed that the mass ratio of organic peroxides to total SOA was 16–18 wt %. This result qualitatively supports the reaction scheme 2B. Johnson et al. employed a chemical-reaction model^{8,33} in which organic peroxides, assumed to be produced in the gas phase, are absorbed on the SOA and then react with carbonyl compounds in the aerosol phase to form peroxy hemiacetals. Johnson et al. predicted the contribution of peroxy hemiacetals to total SOA at $[\text{NO}_x]_0 = 47$ ppbv to be 73%. Note that this value excludes contributions from unstable O_2 -bridged cyclic monomer compounds, which were among the products predicted by Johnson et al. The predicted result is higher than the mass ratio determined in our experiments if the mass ratio is independent of the initial NO_x concentration. Organic peroxides produced in our study may have dissociated during both irradiation and pretreatments. Surratt et al. suggested that about half of the organic peroxides present in SOA were photolyzed during irradiation for 12 h.²⁰ However, our SOA sample was collected within about 2 h of SOA formation, so the loss of organic peroxides by photolysis should be negligible in our study. Docherty et al., who employed the same pretreatment procedure as we did, successfully quantified organic peroxides as contributing 98 ± 7 wt % of the aerosols.²¹ The

Scheme 6a (Formation of C₇ dicarboxylic acid: three-step pathway)**Scheme 6b (Formation of C₇ dicarboxylic acid: two-step pathway)****Scheme 7 (Formations of diphenyl ether-type dimer in the aerosol phase)****Figure 12.** Reaction mechanisms for formation of C₇ unsaturated oxacyclic compounds and diphenyl-ether-type dimers.

loss of organic peroxides after collections of SOA in this study is also negligible. The overestimation of peroxy hemiacetals by the model implies that other low-volatility compounds contribute to the formation of SOA during oxidation of toluene.

In this study, the compounds assigned to C₇ unsaturated oxacyclic oxocarboxylic acids and C₇ unsaturated oxacyclic dicarboxylic acids were found as abundant low-volatility products. Dicarboxylic acids are known to be produced through either the reactions of OH radicals with oxocarboxylic acids or the ozonolyses of cycloalkenes, although the mechanisms of formation of products from the ozonolyses of cycloalkenes have not been established. The two-step oxidations of C₇ unsaturated epoxy dialdehyde (first-generation product i in Figure 1) may give three-membered ring isomers of the C₇ unsaturated oxacyclic dicarboxylic acids, as shown in reaction scheme 6a in Figure 12. However, the dicarboxylic acid compounds must be minor products in this reaction mechanism, because they are third-generation products. The fact that the mass peak of C₇ unsaturated oxacyclic dicarboxylic acids is detected as one of the highest peaks in the mass spectrum of SOA suggests that these products are produced by the reactions of first-generation cycloalkene products with O₃ (i.e., reaction scheme 2A). If toluene oxide (product f in Figure 1) and its isomers react with O₃, then the C₇ dicarboxylic acids found in this study may be produced as shown in reaction scheme 6b of Figure 12. However, the yields of toluene oxides during the toluene oxidation and the O₃ reactivities of toluene oxides have not yet been elucidated. Further experimental studies are necessary to understand the mechanism of formation of the C₇ carboxylic acid products.

4.3. Aerosol-Phase Chemistry. Jang et al. predicted that alcohol and aldehyde products absorbed on aerosols react in the aerosol phase, leading to the formation of hemiacetals.³⁴ In the present study, a group of peaks showing regular mass differences of 14, 16, and 18 were found in the region of $m/z = 200$ –500 of the mass spectra of the SOA sample. However, a negligible number of peaks were observed in the region of $m/z > 200$ of the mass spectrum of the standard mixed sample. The ions of $m/z > 200$ detected in the present SOA sample are not adduct ions produced by the ionization of the analytes. Many compounds assigned to ring-cleavage C₄–C₆ products containing carbonyl and hydroxyl groups were found by the present LCMS-IT-TOF analysis. Although most of these compounds could have been absorbed from the gas phase during filter sampling, these gas-phase products could contribute to the formations of hemiacetal and peroxy hemiacetal oligomers through heterogeneous reactions. The ions of $m/z > 200$ were attributed to hemiacetal oligomers and/or decomposition products of peroxy hemiacetal oligomers. The present results on oligomeric compounds support also the assumptions made in the chemical model of Johnson et al.⁸

The isomers of a diphenyl-ether-type dimer were tentatively identified as products in the present analysis. The signal intensity of a diphenyl-ether-type dimer was ~4% of that of 4-nitro-*o*-cresol (Figure 10); this suggests that this dimer is a minor product. Poly(phenylene ethers) are known to be produced by oxidative coupling polymerization of phenols in solution.³⁰ The formation of the diphenyl-ether-type dimer indicates that phenoxy-type radicals are produced by oxidation of nitrocresol monomers in the aerosol phase. The oxidation of nitrocresols in the solution phase proceeds by reactions with OH radicals.¹ Surratt et al. suggested that organic peroxides in the aerosol phase are photolyzed during photoirradiation.²⁰ This implies that photolysis of organic peroxides, leading to the formation of OH and RO radicals, operates as an initiation step for chain reactions in the aerosol phase. The diphenyl-ether-type dimer found in this study may be produced by the oxidative coupling polymerization of nitrocresols initiated by photolysis of organic peroxides in the aerosol phase (reaction scheme 7 in Figure 12). Forstner et al. suggested that succinic anhydride found in SOA is produced by radical reactions in the aerosol phase (reaction scheme 7 in Figure 12).⁹ The photolysis of maleic anhydride in the aerosol phase leads to the formation of cyclic

biradicals (C(O)C(*)H – C(*)HC(O)O). Succinic anhydride is produced through the two-step hydrogen abstractions by this cyclic biradical from other compounds present in SOA (e.g., nitrocresols). The fact that succinic anhydride is found in the SOA provides additional evidence to show that radical reactions occur in the aerosol phase.

4.4. Generation Depth of Products in SOA. The first-generation products of the toluene oxidation (products shown in Figure 1) are barely absorbed on the aerosol because of their high volatilities. The products identified in SOA in this study were the second- and third-generation products. From the above discussions, we conclude that the major chemical constituents of the aerosol are hemiacetal and peroxy hemiacetal oligomers and low-molecular-weight dicarboxylic acids. It is likely that C₇ unsaturated oxacyclic oxocarboxylic acids and C₇ unsaturated oxacyclic dicarboxylic acids are second-generation products rather than third-generation products. The hemiacetal and peroxy hemiacetal oligomers may be produced by the aerosol-phase reactions of second-generation products. The present results suggest that the major products in the aerosol are second-

generation products and oligomeric compounds produced by heterogeneous reactions of second-generation products.

5. Conclusions

In this study, the chemical compositions of the SOA produced during the photooxidation of toluene were studied at $[\text{NO}]_0 = 0.2$ and 1 ppmv. Fifteen semivolatile products, including ring-cleavage and aromatic compounds, were quantified. The aromatic and ring-cleavage products were found in high abundances at $[\text{NO}]_0 = 1$ and 0.2 ppmv, respectively. The reactions of the OH–aromatic adduct with O_2 and NO_2 explain our observed product distribution. However, the products quantified in this study comprised only a small portion of the aerosol. The SOA yield, the ratio of organic peroxides to total SOA, and the density of SOA were independent of the initial NO concentration, suggesting that the reaction mechanisms for the formation of major SOA products at $[\text{NO}]_0 = 0.2$ and 1 ppmv are basically the same. The reaction channel contributing to the formation of SOA at both of the NO_x levels is the reaction of the OH–aromatic adduct with O_2 . The negative-ion mass spectra of the SOA samples showed that the ion signals attributed to hemiacetal oligomers and/or the decomposition products of peroxy hemiacetal oligomers were detected in the range of $m/z = 200$ –500. The highest mass signals were detected at $m/z = 155$ and 177 and tentatively assigned to C_7 unsaturated oxacyclic oxocarboxylic acids and C_7 unsaturated oxacyclic dicarboxylic acids, respectively. We conclude that the major chemical constituents of the aerosol are hemiacetal and peroxy hemiacetal oligomers and low-molecular-weight dicarboxylic acids. It is likely that peroxy hemiacetal oligomers and dicarboxylic acids are products formed by heterogeneous reactions of second-generation products and second-generation products, respectively.

Acknowledgment. This work was supported by a Grant-in-Aid for Scientific Research from the Ministry of Education, Culture, Sports, Science, and Technology of Japan and a Global Environment Research Fund Project from the Ministry of the Environment of Japan. K.S. thanks Dr. Satoshi Yamaki of the Shimadzu Corporation for the high-resolution mass analysis of the standard and aerosol samples.

References and Notes

- (1) Calvert, J. G.; Atkinson, R.; Becker, K. H.; Kamens, R. M.; Seinfeld, J. H.; Wallington, T. J.; Yarwood, G. *The Mechanisms of Atmospheric Oxidation of Aromatic Hydrocarbons*; Oxford University Press: New York, 2002.
- (2) Izumi, K.; Fukuyama, T. *Atmos. Environ., Part A* **1990**, *24*, 1433.
- (3) Kanakidou, M.; Seinfeld, J. H.; Pandis, S. N.; Barnes, I.; Dentener, F. J.; Facchini, M. C.; Van Dingenen, R.; Ervens, B.; Nenes, A.; Nielsen, C. J.; Swietlicki, E.; Putaud, J. P.; Balkanski, Y.; Fuzzi, S.; Horth, J.;

- Mootgat, G. K.; Winterhalter, R.; Myhre, C. E. L.; Tsigaridis, K.; Vignati, E.; Stephanou, E. G.; Wilson, J. *Atmos. Chem. Phys.* **2005**, *5*, 1053.
- (4) Odum, J. D.; Jungkamp, T. P. W.; Griffin, R. J.; Forstner, H. J. L.; Flagan, R. C.; Seinfeld, J. H. *Environ. Sci. Technol.* **1997**, *31*, 1890.
- (5) Bowman, F. M.; Odum, J. R.; Seinfeld, J. H. *Atmos. Environ.* **1997**, *23*, 3921.
- (6) Hurley, M. D.; Sokolov, O.; Wallington, T. J.; Takekawa, H.; Karasawa, M.; Klotz, B.; Barnes, I.; Becker, K. H. *Environ. Sci. Technol.* **2001**, *35*, 1358.
- (7) Sato, K.; Klotz, B.; Hatakeyama, S.; Imamura, T.; Washizu, Y.; Matsumi, Y.; Washida, N. *Bull. Chem. Soc. Jpn.* **2004**, *77*, 667.
- (8) Johnson, D.; Jenkin, M. E.; Wirtz, K.; Reviejo, M. M. *Environ. Chem.* **2004**, *1*, 150.
- (9) Forstner, H. J. L.; Flagan, R. C.; Seinfeld, J. H. *Environ. Sci. Technol.* **1997**, *31*, 1345.
- (10) Jang, M.; Kamens, R. M. *Environ. Sci. Technol.* **2001**, *35*, 3626.
- (11) Edney, E. O.; Driscoll, D. J.; Weathers, W. S.; Kleindienst, T. E.; Conner, T. S.; McIver, C. D.; Li, W. *Aerosol Sci. Technol.* **2001**, *35*, 998.
- (12) Hamilton, J. F.; Webb, P. J.; Lewis, A. C.; Reviejo, M. M. *Atmos. Environ.* **2005**, *39*, 7263.
- (13) Koehler, C. A.; Fillo, J. D.; Ries, K. A.; Sanchez, J. T.; De Haan, D. O. *Environ. Sci. Technol.* **2004**, *38*, 5064.
- (14) Kalberer, M.; Paulsen, D.; Sax, M.; Steinbacher, M.; Dommen, J.; Prevot, A. S. H.; Fisseha, R.; Weingartner, E.; Frankevich, V.; Zenobi, R.; Baltensperger, U. *Science* **2004**, *303*, 1659.
- (15) Gao, S.; Keywood, M.; Ng, N. L.; Surratt, J.; Varutbangkul, V.; Bahreini, R.; Flagan, R. C.; Seinfeld, J. H. *J. Phys. Chem. A* **2004**, *108*, 10147.
- (16) Guzmán, M. I.; Colussi, A. J.; Hoffmann, M. R. *J. Phys. Chem. A* **2006**, *110*, 3619.
- (17) Doerge, D. R.; Bajic, S. *Rapid Commun. Mass Spectrom.* **1992**, *6*, 663.
- (18) Gayer, R.; Saunders, G. A. *J. Chromatogr.* **1986**, *368*, 456.
- (19) Dahalin, J.; Karlsson, D.; Skarping, G.; Dalene, M. *J. Environ. Monitor.* **2004**, *6*, 624.
- (20) Surratt, J. D.; Murphy, S. M.; Kroll, J. H.; Ng, N. L.; Hildebrandt, L.; Sorooshian, A.; Szmigielski, R.; Vermeylen, R.; Maenhaut, W.; Claeys, M.; Flagan, R. C.; Seinfeld, J. H. *J. Phys. Chem. A* **2006**, *110*, 9665.
- (21) Docherty, K. S.; Wu, W.; Lim, Y. B.; Ziemann, P. *J. Environ. Sci. Technol.* **2005**, *39*, 4049.
- (22) Akimoto, H.; Hoshino, M.; Inoue, G.; Sakamaki, F.; Washida, N.; Okuda, M. *Environ. Sci. Technol.* **1979**, *13*, 471.
- (23) Sato, K.; Klotz, B.; Taketsugu, T.; Takayanagi, T. *Phys. Chem. Chem. Phys.* **2004**, *6*, 3969.
- (24) Bandow, H.; Washida, N.; Akimoto, H. *Bull. Chem. Soc. Jpn.* **1985**, *58*, 2531.
- (25) Sato, K. *Chem. Lett.* **2005**, *34*, 1584.
- (26) Chan, W. H.; Wu, X. *J. Analyst* **1998**, *123*, 2851.
- (27) Banerjee, D. K.; Budke, C. C. *Anal. Chem.* **1964**, *36*, 792.
- (28) Hay, A. S.; Balchard, H. S.; Endres, G. F.; Eustance, J. W. *J. Am. Chem. Soc.* **1959**, *81*, 6335.
- (29) Yamashita, Y.; Ouchi, K. *Carbon* **1981**, *19*, 89.
- (30) Raoult, S.; Rayez, M. T.; Rayez, J. C.; Lesclaux, R. *Phys. Chem. Chem. Phys.* **2004**, *6*, 2245.
- (31) Knispel, R.; Koch, R.; Siese, M.; Zetzsch, C. *Ber. Bunsen-Ges. Phys. Chem.* **1990**, *94*, 1375.
- (32) Atkinson, R.; Aschmann, S. M.; Arey, J.; Carter, W. P. L. *Int. J. Chem. Kinet.* **1989**, *21*, 801.
- (33) Stroud, C. A.; Maker, P. A.; Michelangeli, D. V.; Mozurkewich, M.; Hastie, D. R.; Barbu, A.; Humble, J. *Environ. Sci. Technol.* **2004**, *38*, 1471.
- (34) Jang, M. S.; Czoschke, N. M.; Lee, S.; Kamens, R. M. *Science* **2002**, *298*, 814.